

Effects of spin-orbit interactions on tunneling via discrete energy levels in metal nanoparticles

D. G. Salinas, S. Guéron, and D. C. Ralph

Laboratory of Atomic and Solid State Physics, Cornell University, Ithaca, New York 14853

C. T. Black

IBM Thomas J. Watson Research Center, Yorktown Heights, New York 10598

M. Tinkham

Department of Physics and Division of Applied Sciences, Harvard University, Cambridge, Massachusetts 02138

(Received 19 March 1999)

The presence of spin-orbit scattering within an aluminum nanoparticle affects measurements of the discrete energy levels within the particle by (1) reducing the effective g factor below the free-electron value of 2, (2) causing avoided crossings as a function of magnetic field between predominantly spin-up and predominantly spin-down levels, and (3) introducing magnetic-field-dependent changes in the amount of current transported by the tunneling resonances. All three effects can be understood in a unified fashion by considering a simple Hamiltonian. Spin-orbit scattering from 4% gold impurities in superconducting aluminum nanoparticles produces no dramatic effect on the superconducting gap at zero magnetic field, but we argue that it does modify the nature of the superconducting transition in a magnetic field. [S0163-1829(99)10731-8]

I. INTRODUCTION

For decades, systematic studies of the quantum-mechanical energy levels of atoms and atomic nuclei have provided an understanding of the forces governing these systems. Recently, it has also become possible to measure the discrete “electrons-in-a-box” energy levels within semiconductor quantum dots and metal nanoparticles.¹⁻³ Experiments have shown that different classes of forces and interactions acting on the electrons inside these materials affect the level spectra in distinguishable ways. Therefore, just as in atomic and nuclear physics, the discrete spectra in these condensed matter systems can provide a tool for understanding the interactions which influence electronic structure, uncovering effects that are not clearly visible if the individual quantum levels in the system cannot be resolved. The consequences of superconducting pairing interactions^{4,5} and more general electron-electron interactions^{6,7} have previously been analyzed for the case of aluminum nanoparticles. In this paper, we discuss spin-orbit (SO) interactions, resulting both from accidental defects in the Al nanoparticles and from gold dopants. We examine how SO scattering affects both the energies of the quantum levels and the amount of tunnel current which may be carried by each state. We find that the magnetic-field dependence of these quantities may be understood in a unified fashion within a simple model. The effects of SO scattering on the superconducting properties of an aluminum nanoparticle are also discussed.

The study of SO scattering within metals has a long history. The metal samples of the types traditionally examined are large enough that the electronic states effectively form a continuum. In this case, the quantity of primary experimental interest in SO studies is the rate at which SO interactions cause the spin of an electron assumed to be initially in a pure spin-up or spin-down state to be scattered into continuum states with opposite spin. This rate can be measured using

weak localization experiments for disordered metal samples⁸ or, alternatively, by analyzing the form of the spin-dependent density of states determined by tunneling between thin superconducting films in a parallel magnetic field.⁹ SO interactions are of fundamental theoretical importance because their presence changes the symmetry properties of the Hamiltonian. For instance, the statistics of the energy levels in chaotic time-reversal-symmetric quantum dots are predicted to change from the orthogonal distribution in the absence of SO scattering to the symplectic distribution for a strong SO interaction, with a corresponding increase in the strength of the effective energy-level repulsion.^{10,11} Perhaps the most dramatic consequences of SO coupling in metals occur in ferromagnets, since the SO interaction underlies the phenomena of magnetic anisotropy and the anomalous Hall effect.

An analysis of the effects of SO interactions in metal nanoparticles requires a somewhat different viewpoint than for larger devices with a continuum density of states. Considering basic symmetries, the Hamiltonian operator describing electrons within a metal sample does not commute with the components of the total electronic spin operator in the presence of the SO interaction. This means that it is not possible to construct a set of basis states which are simultaneously eigenstates of both the energy and S_z . The discrete energy eigenstates, through which electron tunneling occurs in a metal nanoparticle, will thus necessarily be linear superpositions of pure spin-up and pure spin-down states, with the extent of admixture determined by the magnitude of SO matrix elements. Because these discrete energy eigenstates defined in the presence of the SO interaction are in fact well-defined energy eigenstates, the SO interaction does not lead to any decrease in their lifetime. For this reason, the experimental quantities of interest in this paper will not be scattering rates, but rather shifts in the energies of the electronic states and changes in the tunneling current carried by the states.¹² Both of these quantities are affected by the extent of

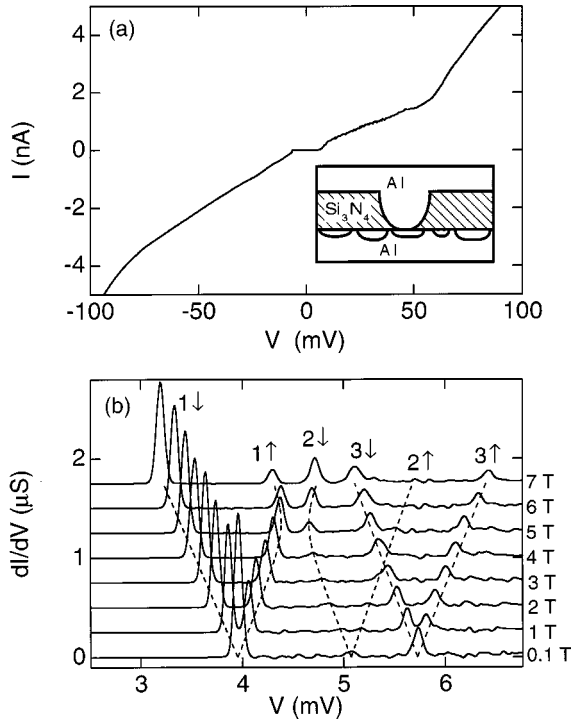


FIG. 1. (a) Large-scale Coulomb-staircase curve for a tunneling device containing a nm-scale Al particle at $T=50$ mK. Inset: Cross-sectional device schematic. (b) Tunneling spectrum of discrete state resonances in the same sample, for a range of applied magnetic fields, at $T=50$ mK. The curves are offset in dI/dV for visibility. Orbital state no. 2 gives small but visible resonances at low B . Small changes in offset charge occurred between the 6 and 7 T scans and between the 6 and 7 T scans, shifting peak positions. The 0.1 and 7 T scans have therefore been shifted along the voltage axis, to give the best fit to a linear dependence for peak $1\downarrow$. Dotted lines are guides to the eye.

admixture of spin-up and spin-down components within the energy eigenstates. An initial analysis of some of the results we will discuss has appeared previously.¹³

The measurements we describe were performed using tunneling devices containing an Al particle less than 10 nm in diameter, connected to Al electrodes via aluminum oxide tunnel junctions. A device schematic is shown in the inset to Fig. 1(a). The fabrication steps have been described in detail previously.³ An aluminum electrode is first deposited on one side of an insulating silicon nitride membrane containing a 10-nm-scale through hole. The Al is oxidized to form a nm-scale tunnel junction near the base of the hole. A layer of Al nanoparticles is then formed on the other side of the membrane by depositing 2.5 nm of Al, which balls up into small particles due to surface tension. In some of the devices described in this paper, the Al evaporation for the particles was interrupted halfway through and a thin layer of gold was deposited to give roughly a 4% (atomic) dose of Au inside the nanoparticle. Since Al and Au are sufficiently miscible to form several intermetallic compounds,¹⁴ and both have significant surface mobilities on the nm length scale, we expect that the two types of atoms will be intermixed. When the nanoparticle deposition is complete, their surfaces are oxidized to form tunnel junctions, and a thick aluminum film is deposited as a second electrode. Devices in which tunneling occurs via a single nanoparticle joining the two leads are

selected based on the measurement of a ‘‘Coulomb-staircase’’ current-voltage curve [Fig. 1(a)].

II. EFFECTS OF SPIN-ORBIT INTERACTIONS ON DISCRETE STATES

Tunneling spectra of the discrete energy levels are shown in Fig. 1(b), at different values of the applied magnetic field, for an Al particle in which we will identify the presence of spin-orbit scattering. This particle is nominally pure Al, but we have also observed all the features that we will ascribe to SO scattering in Au-doped particles. We speculate that the source of the SO scattering in the nominally pure Al particle is an unintended defect or impurity. Each peak in the dI/dV vs voltage spectrum corresponds to the threshold for electron tunneling via a different quantum-mechanical state in the particle, each with the same number of electrons (either one more or one less than in the $V=0$ ground state of the particle). In order to convert from the voltage scale to the true energy within the nanoparticle, it is necessary to determine the ratio of the capacitances of the particle to the two electrodes, C_1/C_2 . This is measured most accurately either by comparing the positions of the tunneling peaks due to the same state at opposite signs of bias voltage, or by measuring shifts in peak positions for superconducting vs normal-state electrodes.³ The conversion factor from voltage to energy for the data of Fig. 1(b) is $eC_1/(C_1+C_2)=e(0.53\pm 0.01)$. A rough estimate of the volume of the particle can be made based on the capacitances of the particle, determined from the spacing between steps in the Coulomb-staircase curve, $\Delta V=e/C_{\text{smaller}}=78$ mV. Together with the known capacitance per unit area of oxidized aluminum tunnel junctions, ~ 50 fF/ μm^2 ,¹⁵ and assuming a particle shape that is approximately a hemisphere, we estimate a particle radius of approximately $r=3$ nm for this device.

The peaks in Fig. 1(b) have many features qualitatively similar to previous studies of tunneling resonances in pure Al. As the applied magnetic field (B), applied parallel to the plane of the Si_3N_4 membrane in the device, is increased from low-field values, each peak splits in two, and the energy difference between these pairs increases linearly with B' at low B [Fig. 2(a)].¹⁶ This can be understood as Zeeman splitting of the energies of the predominantly spin-up and spin-down states associated with each orbital eigenstate. The observation of tunneling via both of the Zeeman-split states for the lowest-energy tunneling state (no. 1) indicates that the tunneling transition corresponds to a change from an even number to an odd number of electrons within the nanoparticle.³ Within the uncertainties of the measurement, the splitting is symmetric around the low-field resonance energy, with little shift up or down for the average of the Zeeman-split peaks.¹⁷ This indicates that the effect of B' on the orbital component of the electronic energy is much weaker than on the spin component. This is not surprising, due to the particle’s small size and disorder. Because any real nanoparticle will not have a spherical shape or a smooth surface, the orbital angular momentum of the eigenstates will be quenched to zero in the absence of an applied field. In this situation, the correlation scale which describes the effect of the magnetic field on the energy eigenstates is expected to be on the order of $\Phi_0\sqrt{\delta/E_{\text{Th}}}/r^2$, where Φ_0 is the flux quantum,

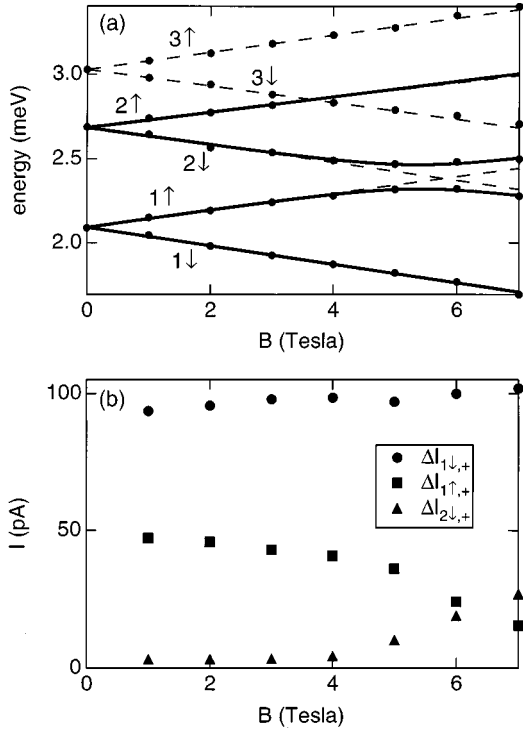


FIG. 2. (a) Energies of the discrete electronic states within the nanoparticle of Fig. 1, calculated by multiplying the voltage positions of the resonances by the capacitance ratio $eC_1/(C_1 + C_2) = e0.53$. Dashed lines are extensions of the low-field linear dependence of the energies on B . Solid lines show the result of the spin-orbit interaction model, describing the avoided crossing between levels $1\uparrow$ and $2\downarrow$. (b) Magnitude of the current increments contributed by each of the first three resonances for positive voltage bias. [Equal to the area under the peaks in Fig. 1(b).] Note the crossover in magnitude for the current increments associated with states $1\uparrow$ and $2\downarrow$.

δ is the mean level spacing, and $E_{\text{Th}} \approx \hbar v_F / (2r)$ is the Thouless energy scale for a ballistic sample.¹⁸ For a particle with radius 3 nm the expected field correlation scale is approximately 30 T. Since this is much larger than the fields of interest in our experiment, throughout the paper we will assume that the effect of B on the orbital eigenstates within the particle is negligible, so as to concentrate on spin effects.

There are at least three features of the data in Figs. 1(b) and 2(a) that differ from typical Al particles. First, let us define an effective g factor such that the energy splitting between Zeeman-split states is $\Delta E = g_{\text{eff}} \mu_B B$ (to linear order in B), where μ_B is the Bohr magneton. In over 80% of the nominally pure Al samples we have examined previously, $g_{\text{eff}} = 2 \pm 0.05$, which is as expected, because SO scattering is negligible in pure Al, and the free-electron g factor should apply.¹⁰ In the sample in question, however, g_{eff} is significantly less, and it varies from peak to peak: $g_{\text{eff}} = 1.84 \pm 0.03$, 1.68 ± 0.08 , and 1.76 ± 0.05 for the three resonances in Fig. 2(a). The second difference between this sample and past measurements concerns level crossings. In pure Al particles with g factors approximately equal to 2 we have not observed departures from linear Zeeman splittings when spin-up and spin-down levels corresponding to different orbital states cross as a function of B . For a sample without SO scattering, this must be the case, for then there is no coupling

between spin-up and spin-down states in the Hamiltonian. In contrast, the Zeeman splittings of the first two orbital states shown in Figs. 1(b) and 2(a) show a clear departure from linear behavior, because the upward-trending level from the first state ($1\uparrow$) undergoes an avoided crossing with the downward-trending level from the second state ($2\downarrow$). The third difference is that the amplitudes of the resonances for the sample in question show unusual features. Whereas in most Al particles the amplitudes of the resonances do not display any significant B dependence, here the amplitudes of the two levels undergoing the avoided crossing change dramatically, with the higher-amplitude resonance shrinking and the smaller-amplitude resonance growing in the avoided-crossing region. The amount of current contributed by each resonance is plotted in Fig. 2(b), where it can be seen that the sum of the current increments contributed by these two resonances is approximately constant.

All of these features can be understood by considering the Hamiltonian of the electrons in the presence of SO scattering. The theory behind the physics of the g factor has been considered previously.^{19,10} Let us write the Hamiltonian in zero magnetic field as

$$H = H_0 + H_{\text{SO}}, \quad (1)$$

where H_{SO} contains the terms that couple spin-up states to spin-down states, and H_0 describes all the spin-independent forces and interactions. We will neglect the effect of the magnetic field on electron orbits, and assume that the sample contains no magnetic impurities. Let $|A_{n\uparrow}\rangle$ and $|A_{n\downarrow}\rangle$ represent the unperturbed eigenstates of H_0 . Then, performing perturbation theory to lowest order in H_{SO} , the (not normalized) eigenstates of the full Hamiltonian have the form

$$|\Phi_{n''\uparrow n}\rangle = |A_{n\uparrow}\rangle + \sum_{m \neq n} \frac{\langle A_{m\downarrow} | H_{\text{SO}} | A_{n\uparrow} \rangle |A_{m\downarrow}\rangle}{E_n - E_m}. \quad (2)$$

The spin-orbit interaction causes the eigenstates to consist of a linear superposition of spin-up and spin-down states; hence the notation “ \uparrow ” reflects that the eigenstate can be considered at most predominantly spin up. The effective g factor for state n may be written¹⁰

$$g_{\text{eff},n} \equiv 2 \frac{\langle \Phi_{n''\uparrow n} | \sigma_z | \Phi_{n''\uparrow n} \rangle}{\langle \Phi_{n''\uparrow n} | \Phi_{n''\uparrow n} \rangle} = 2 \left(1 - 2 \sum_{m \neq n} \frac{|\langle A_{m\downarrow} | H_{\text{SO}} | A_{n\uparrow} \rangle|^2}{(E_n - E_m)^2} \right). \quad (3)$$

(Evaluating this expression for the “ \downarrow ” state gives the same answer.) The meaning of Eq. (3) is that g_{eff} is reduced below the free-electron value of 2 by an amount determined by the extent to which SO matrix elements couple the state n to other states m of opposite spin. Because the energy eigenstates are no longer purely spin up or spin down in the presence of spin-orbit interactions, they respond more weakly to an applied magnetic field than pure-spin states. Next consider the nature of the matrix elements $|\langle A_{m\downarrow} | H_{\text{SO}} | A_{n\uparrow} \rangle|^2$. Due to the chaotic and strongly fluctuating character of the wave functions in a metallic nanoparticle,⁶ the magnitudes of these factors will be strongly varying for different values of m and n , depending on the details of the wave function over-

laps at the positions of the SO scattering defects. Therefore, from Eq. (3), it can be seen that different energy levels in the same sample may have different values of g_{eff} , as we observe. Because of the form of the denominator in the second term of Eq. (3), we can also expect that matrix elements which couple eigenstates nearby in energy will produce the strongest influence on g_{eff} . We will demonstrate an example of this below.

Let us now begin to analyze the variations in the level energies and the currents carried by the particular levels displayed in Fig. 2. To do this we will write explicitly the form of the effective Hamiltonian matrix for just the four energy levels associated with the first two orbital states, which we label as $|a\downarrow\rangle$, $|a\uparrow\rangle$, $|b\downarrow\rangle$, and $|b\uparrow\rangle$. The most convenient set of basis states are those which diagonalize the spin-independent part of the Hamiltonian H_0 together with all of H_{SO} except that term which couples states $|a\rangle$ and $|b\rangle$ to each other. (With this choice, the basis states are already not purely spin up or spin down, so the arrows should henceforth be understood to mean predominantly spin up or predominantly spin down.) The SO interaction is invariant upon time reversal. The most general Hamiltonian satisfying this symmetry, including both ordinary potential scattering and SO scattering, and describing two Kramers doublets in the absence of an applied magnetic field is (with the above basis choice) represented by the matrix¹¹

$$H = \begin{pmatrix} E_{a\downarrow} & 0 & d & c \\ 0 & E_{a\uparrow} & -c^* & d^* \\ d^* & -c & E_{b\downarrow} & 0 \\ c^* & d & 0 & E_{b\uparrow} \end{pmatrix}. \quad (4)$$

The placement of the zero elements and the arrangement of the elements involving c and d are required so that the Kramers doublets are in fact degenerate at $B=0$. The matrix element $d = \langle a\downarrow | H_{\text{SO}} | b\downarrow \rangle$ couples states of the same spin, so that it is equivalent to ordinary potential scattering for our purposes. Without loss of generality, we can pick the orbital basis states $|a\rangle$ and $|b\rangle$ so that $d=0$. We identify $c = \langle a\downarrow | H_{\text{SO}} | b\uparrow \rangle$. Because we are assuming that the orbital states are not modified by a magnetic field, we take the matrix element c to be independent of B . The only B dependence then left in the problem is due to the influence of the Zeeman energies in the diagonal terms of the Hamiltonian. We write these Zeeman energies by including effective g factors, g'_{eff} , for the spin and, simply for convenience in the fitting, we also allow a linear term $g_{\text{orb}}\mu_B B$ (where μ_B is the Bohr magneton) to model any shift in the average energy of the Zeeman-split pairs. (We will see that the fits give $g_{\text{orb}} \approx 0$.) With these assumptions, the diagonal terms as a function of B are

$$E_{a\uparrow,\downarrow} = E_a + \left(g_{\text{orb},a} \pm \frac{g'_{\text{eff},a}}{2} \right) \mu_B B, \\ E_{b\uparrow,\downarrow} = E_b + \left(g_{\text{orb},b} \pm \frac{g'_{\text{eff},b}}{2} \right) \mu_B B. \quad (5)$$

The terms $g'_{\text{eff},a}$ and $g'_{\text{eff},b}$ must take into account the SO coupling of state $|a\rangle$ or $|b\rangle$ to all states except each other, so

that these terms will not be equal to 2. Instead, from Eq. (3), we should expect that $g'_{\text{eff},a}$ and $g'_{\text{eff},b}$ will be related to the total effective g factor by the relationship

$$g'_{\text{eff}} = g_{\text{eff}} + 4 \frac{|\langle a\downarrow | H_{\text{SO}} | b\uparrow \rangle|^2}{(E_a - E_b)^2}. \quad (6)$$

With $d=0$, Eq. (4) gives a very simple Hamiltonian, consisting of two separate 2×2 matrices coupling $|a\downarrow\rangle$ to $|b\uparrow\rangle$, and $|a\uparrow\rangle$ to $|b\downarrow\rangle$.

For a weak SO interaction, $|\langle a\downarrow | H_{\text{SO}} | b\uparrow \rangle| \ll E_b - E_a$, the effects of the interaction are easy to understand. Away from any degeneracies among the diagonal terms, the energy eigenvalues will be approximately equal to the diagonal terms, except for a shift in the effective g factor. When the Zeeman energies are such that two diagonal energies approach degeneracy, they will exhibit a simple avoided crossing of magnitude equal to $2|\langle a\downarrow | H_{\text{SO}} | b\uparrow \rangle|$, because this term couples the two states. Solving the Hamiltonian explicitly (with $d=0$), the model produces an excellent fit for the B dependence of the measured levels [Fig. 2(a)], with the parameters $|\langle a\downarrow | H_{\text{SO}} | b\uparrow \rangle| = 73 \pm 4 \mu\text{eV}$, $g'_{\text{eff},a} = 1.90 \pm 0.04$, $g'_{\text{eff},b} = 1.74 \pm 0.04$, $g_{\text{orb},a} = -0.03 \pm 0.04$, and $g_{\text{orb},b} = -0.10 \pm 0.06$. The difference between the directly measured g values $g_{\text{eff},1} = 1.84 \pm 0.03$, $g_{\text{eff},2} = 1.68 \pm 0.08$ on the one hand and the fitting terms $g'_{\text{eff},a}$, $g'_{\text{eff},b}$ on the other is consistent with Eq. (6), since $4|\langle a\downarrow | H_{\text{SO}} | b\uparrow \rangle|^2 / (E_a - E_b)^2 = 0.06$. From this we can see that the SO coupling between states $|a\rangle$ and $|b\rangle$ contributes approximately 40% of the reduction from $g_{\text{eff}}=2$ for the orbital state 1, and 20% for state 2. SO coupling to other states must account for the remainder. The fact that we do not have the sensitivity to resolve any avoided crossing between the states $2\uparrow$ and $3\downarrow$ [Fig. 2(a)] indicates that the SO matrix element coupling these states is smaller than $|\langle a\downarrow | H_{\text{SO}} | b\uparrow \rangle|$.

The changes in the amount of current carried by the resonances [Fig. 2(b)] can be understood by examining the manner in which the energy eigenstates are composed of linear superpositions of basis states. Consider the two energy eigenstates ($|\text{lower}\rangle$ and $|\text{upper}\rangle$) formed from superpositions of the avoided-crossing basis states $|a\uparrow\rangle$ and $|b\downarrow\rangle$. By diagonalizing the Hamiltonian [Eq. (4) with $d=0$], it is simple to demonstrate that these have the form

$$|\text{lower}\rangle = \gamma(B)|a\uparrow\rangle + \eta(B)|b\downarrow\rangle, \\ |\text{upper}\rangle = -\eta^*(B)|a\uparrow\rangle + \gamma^*(B)|b\downarrow\rangle, \quad (7)$$

where the coefficients $\gamma(B)$ and $\eta(B)$ depend on B as shown in Fig. 3(a). The key point is that, as the magnetic field is varied in the avoided-crossing region, the relative contributions of $|a\uparrow\rangle$ and $|b\downarrow\rangle$ to each eigenstate will change, and consequently the tunneling currents can be altered. This simple conclusion will be the topic of the next several pages of discussion. The reason for an extended analysis is that the magnitudes of the currents are determined by a process of sequential tunneling across the two tunnel junctions in the device, so that the measured current values are not simply a function of the tunneling rate into an individual energy eigenstate. Instead, the current will be affected by all energetically allowed transitions within the device. In order to deal with this complication, the plan of our discussion is that

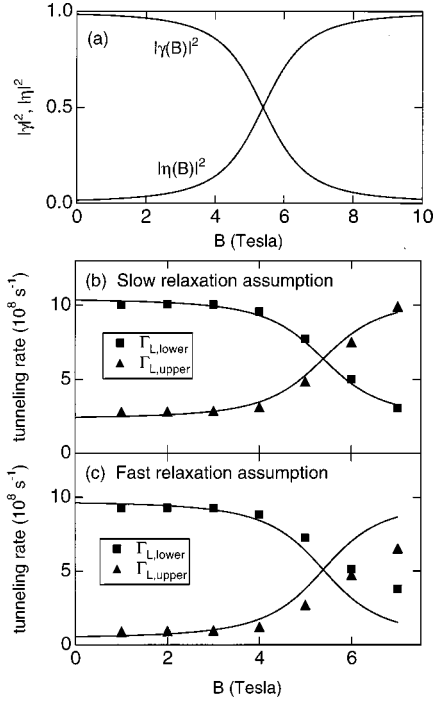


FIG. 3. (a) Magnetic-field dependence of the coefficients in Eq. (9), for the superposition of predominantly spin-up and spin-down basis states occurring in the avoided crossing of levels $1\uparrow$ and $2\downarrow$. (b) and (c) Markers: Tunneling rates for the energy eigenstates in the avoided-crossing region, estimated as discussed in the text using either Eq. (11) or Eq. (12), assuming that the relaxation rate of nonequilibrium excitations within the particle is either slower or faster than the tunneling rates. Lines: Fits using the predictions of the spin-orbit Hamiltonian. Regardless of the energy-relaxation rate, the magnetic-field-dependent changes in the currents flowing via the levels in the avoided-crossing region [Fig. 2(b)] can be explained qualitatively by the change in tunneling rates expected from the SO Hamiltonian.

we will focus first on the bare tunneling rates $\Gamma_{L,lower}$, $\Gamma_{L,upper}$, $\Gamma_{R,lower}$, and $\Gamma_{R,upper}$ for tunneling of an electron between the energy eigenstates ($|\text{lower}\rangle$ and $|\text{upper}\rangle$) and the left (L) and right (R) electrodes. Later we will examine two different limits for calculating the total current through the device in terms of these bare tunneling rates. In either case we will see that, despite the complications, the changes in the total current carried by a particular tunneling resonance as a function of magnetic field can be related to the changing composition of the energy eigenstates in the avoided-crossing region [Eq. (7)].

For the high-resistance barriers used in the experiment, the bare tunneling rates between either of the electrodes and energy levels in the nanoparticle can be written in terms of matrix elements of a tunneling Hamiltonian H_T which couples states in the electrodes to the energy eigenstates. Since tunneling of a spin-up electron from the electrode is necessarily incoherent with respect to tunneling of a spin-down electron, we have for the left junction (for the right junction the equations are similar)

$$\Gamma_{L,lower} = \frac{2\pi}{\hbar} \sum_{\psi \text{ in left electrode}} \{ |\langle \psi_{\text{electrode},\uparrow} | H_T | \text{lower} \rangle|^2 + |\langle \psi_{\text{electrode},\downarrow} | H_T | \text{lower} \rangle|^2 \},$$

$$\Gamma_{L,upper} = \frac{2\pi}{\hbar} \sum_{\psi \text{ in left electrode}} \{ |\langle \psi_{\text{electrode},\uparrow} | H_T | \text{upper} \rangle|^2 + |\langle \psi_{\text{electrode},\downarrow} | H_T | \text{upper} \rangle|^2 \}. \quad (8)$$

These expressions can be given in a more illuminating form by writing $|\text{lower}\rangle$ and $|\text{upper}\rangle$ explicitly as linear superpositions of the basis states $|a\uparrow\rangle$ and $|b\downarrow\rangle$ [as in Eq. (7)]. The tunneling rates become

$$\begin{aligned} \Gamma_{L,lower} &= |\gamma(B)|^2 \Gamma_{L,a\uparrow} + |\eta(B)|^2 \Gamma_{L,b\downarrow}, \\ \Gamma_{L,upper} &= |\eta(B)|^2 \Gamma_{L,a\uparrow} + |\gamma(B)|^2 \Gamma_{L,b\downarrow}, \end{aligned} \quad (9)$$

where the B -independent tunnel-coupling strengths for the basis states are

$$\begin{aligned} \Gamma_{L,a\uparrow} &= \frac{2\pi}{\hbar} \sum_{\psi} |\langle \psi_{\text{electrode},\uparrow} | H_T | a\uparrow \rangle|^2, \\ \Gamma_{L,b\downarrow} &= \frac{2\pi}{\hbar} \sum_{\psi} |\langle \psi_{\text{electrode},\downarrow} | H_T | b\downarrow \rangle|^2. \end{aligned} \quad (10)$$

For values of B well below the avoided-crossing range, $\gamma(B) \approx 1$, $\eta(B) \approx 0$, and the rates for tunneling into the energy eigenstates are equal to $\Gamma_{L,a\uparrow}$ and $\Gamma_{L,b\downarrow}$. Since in this regime the total current passing through the $|b\rangle$ resonances [orbital state no. 2 in Figs. 1(b), 2(b)] is very small compared to the $|a\rangle$ peaks (orbital state no. 1), clearly these two rates must be very different. As B is swept through the avoided crossing region, the admixture of the two basis states within the eigenstates changes, with $|\gamma(B)|$ evolving gradually from 1 to 0, and $|\eta(B)|$ going from 0 to 1. This means that there should be a gradual exchange of tunneling weight between $|\text{lower}\rangle$ and $|\text{upper}\rangle$, with $\Gamma_{L,lower}$ evolving from $\Gamma_{L,a\uparrow}$ to $\Gamma_{L,b\downarrow}$, and $\Gamma_{L,upper}$ doing the reverse. Qualitatively, this crossover behavior is apparent in the currents in Fig. 2(b).

In order to attempt a more quantitative treatment of the measured currents, it is necessary to analyze the relationship between the bare tunneling rates Γ discussed above, and the value of the current that results from sequential tunneling across the two tunnel barriers. This requires a full consideration of all the processes that can occur during current flow. When the applied bias is larger than the level spacing, non-equilibrium electron distributions are produced within the nanoparticle during tunneling, and these can open new channels for electrons to flow.^{6,20} The idea is shown in Fig. 4. In Fig. 4(a) we show the simple process of an electron tunneling from the left electrode to an empty level on the particle, when the voltage across the device is sufficient to supply the threshold tunneling energy. Due to electrostatic interaction with this additional electron upon its arrival, the lower-energy electronic states already filled within the particle can be shifted up in energy to the positions drawn. If the applied voltage needed to initiate tunneling is larger than the level separation between states, one possibility for the next step in the tunneling process might be as shown in Fig. 4(b), where an electron tunnels out of one of these lower-energy states to the right electrode, leaving an electron-hole excitation on the particle. After this, the excited electron might relax [Fig. 4(c)] before the next electron tunnels onto the particle. Alternatively an electron may tunnel from the left electrode

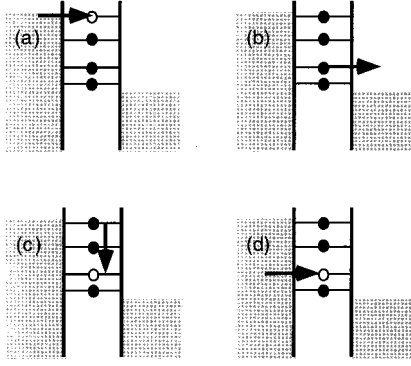


FIG. 4. (a)–(d) Some of the allowed transitions contributing to the magnitude of the current flowing at a tunneling threshold.

into the hole [Fig. 4(d)]. All of these processes, and all other energetically allowed transitions, will contribute to the value of the current that results when the voltage is turned above the threshold required to initiate tunneling in Fig. 4(a). The lower-energy, initially filled states can contribute to the current even though they are hidden in the sense that they do not produce tunneling thresholds of their own. In general, to calculate the total current, one must solve a full master equation which takes into account the rates of all the allowed transitions, including the hidden levels. The parameters entering the calculation are the number of hidden levels, the tunneling rates between each level and the left and right leads, and the relaxation rates for the different allowed excitations within the particle.

For samples of the sort investigated in Figs. 1–3, which do not have a gate electrode that can be used to adjust the number of hidden states, the measured data are not sufficient to fully determine all of the parameters required to describe the currents quantitatively. However, progress can be made with some simplifying assumptions. One particular difficulty is that we do not know how the relaxation rate for excitations within the particle [e.g., Fig. 4(c)] compares to the tunneling rates in this sample. The predicted order of magnitude for the relaxation rate due to electron-phonon scattering is 10^8 s^{-1} ,⁶ less than the tunneling rates we will determine, but only by about a factor of 10. Allowing for some uncertainty in the theory, we will consider both of the two simple limits—that the relaxation rate is either much slower or much faster than the tunneling rate. The following discussion should not be considered a quantitative determination of tunneling parameters, but it will serve to illustrate the way in which the measured changes in current increments as a function of B can be linked to the bare tunneling rates. We also invoke three other simplifying assumptions: (1) that the number of hidden states stays the same over the range of voltage and magnetic field analyzed in Figs. 1(b) and 2, (2) that the ratios $\Gamma_{L,i}/\Gamma_{R,i}$, for the tunneling rates from quantum level i to the left and right electrodes, are all the same, and (3) that for all *hidden* states the tunneling rates to the left electrode are identical $\equiv \Gamma_{L,h}$. We define $x = \Gamma_L/\Gamma_R$. These assumptions reduce the free parameters in the problem to a tractable number, but we make no rigorous claims as to plausibility.

We first consider the slow-relaxation limit, in which we can ignore all processes of the sort pictured in Fig. 4(c). In this limit, the second assumption listed above leads to a great

simplification, because the probability for occupation of any quantum level accessible by tunneling will be the same. If the voltage bias is such that N hidden levels and M originally empty levels participate in tunneling, the total current that results at $T=0$ is, by solution of an elementary set of rate equations, for positive (+) and negative (−) bias,

$$I_{M,N,+} = \frac{eM(N+1)(N\Gamma_{L,h} + \sum_{i=1}^M \Gamma_{L,i})}{(N+M)(N+1+xM)},$$

$$I_{M,N,-} = \frac{eM(N+1)(N\Gamma_{L,h} + \sum_{i=1}^M \Gamma_{L,i})}{x(N+M)(N+1+M/x)}. \quad (11)$$

Within the model, we can determine the values for the four free parameters N , x , $\Gamma_{L,h}$, and $\Gamma_{L,1}$ (the tunneling rate into the lowest-energy initially empty orbital state at low field) from the four low-field ($B=2$ T) values of the total, cumulative currents flowing at the $1\uparrow$ and $1\downarrow$ thresholds, for positive and negative bias: $I_{1,N,+} = \Delta I_{1\downarrow,+} = 9.6 \times 10^{-11}$ A, $I_{2,N,+} = \Delta I_{1\uparrow,+} + \Delta I_{1\downarrow,+} = 1.41 \times 10^{-10}$ A, $I_{1,N,-} = \Delta I_{1\downarrow,-} = 6.6 \times 10^{-11}$ A, and $I_{2,N,-} = \Delta I_{1\uparrow,-} + \Delta I_{1\downarrow,-} = 1.19 \times 10^{-10}$ A. Because of time-reversal symmetry we can assume that $\Gamma_{L,1\uparrow} = \Gamma_{L,1\downarrow}$ for small B . The results for the four free parameters are $N=2.4$, $x=2.0$, $\Gamma_{L,h} = 9.4 \times 10^8 \text{ s}^{-1}$, and $\Gamma_{L,1} = 1.01 \times 10^9 \text{ s}^{-1}$. The fact that N is not an integer may reflect the weaknesses of the assumption that the ratio $x = \Gamma_L/\Gamma_R$ is the same for all the quantum levels and/or the assumption of slow relaxation. Employing these values and the measured (positive-bias) current increments for the avoided-crossing states shown in Fig. 2(b), we can then invert Eq. (11) (for $M=2$ and 3) to estimate the bare tunneling rates $\Gamma_{L,\text{lower}}$ and $\Gamma_{L,\text{upper}}$ over the whole range of B from 1 to 7 T, with the results shown in Fig. 3(b).

In the same way we can consider the fast-relaxation limit, in which the electrons in the nanoparticle relax to their lowest-energy state between all tunneling events. The solutions to the rate equations are

$$I_{M,N,+} = \frac{e(\Gamma_{L,1} + N\Gamma_{L,h})(\sum_{i=1}^M \Gamma_{L,i})}{\Gamma_{L,1} + N\Gamma_{L,h} + x(\sum_{i=1}^M \Gamma_{L,i})},$$

$$I_{M,N,-} = \frac{e(\Gamma_{L,1} + N\Gamma_{L,h})(\sum_{i=1}^M \Gamma_{L,i})}{x[\Gamma_{L,1} + N\Gamma_{L,h} + (\sum_{i=1}^M \Gamma_{L,i})/x]}. \quad (12)$$

In this case there are just three parameters, $\Gamma_{L,1}$, x , and $N\Gamma_{L,h}$, which can be determined from the $B=2$ T values of $I_{1,N,+} = \Delta I_{1\downarrow,+}$, $I_{2,N,+} = \Delta I_{1\uparrow,+} + \Delta I_{1\downarrow,+}$, and $I_{1,N,-} = \Delta I_{1\downarrow,-}$ as $\Gamma_{L,1} = 9.3 \times 10^8 \text{ s}^{-1}$, $x = 1.96$, and $N\Gamma_{L,h} = 2.4 \times 10^9 \text{ s}^{-1}$. These parameters, together with Eq. (12), predict a value of 1.18×10^{-10} A for $I_{2,N,-} = \Delta I_{1\uparrow,-} + \Delta I_{1\downarrow,-}$, in good agreement with the measured value 1.19×10^{-10} A. We can then invert Eq. (12) using the measured current increments of the avoided-crossing states in Fig. 2(b) to estimate the tunneling rates $\Gamma_{L,\text{lower}}$ and $\Gamma_{L,\text{upper}}$ in the fast-relaxation limit [Fig. 3(c)]. The differences between Figs. 3(b) and 3(c) reflect to some extent the degree of uncertainty with which we can estimate these bare tunneling rates.

We see from both Figs. 3(b) and 3(c) that the crossover observed in the magnitude of the current increments for the two avoided-crossing states can be related to a crossover in

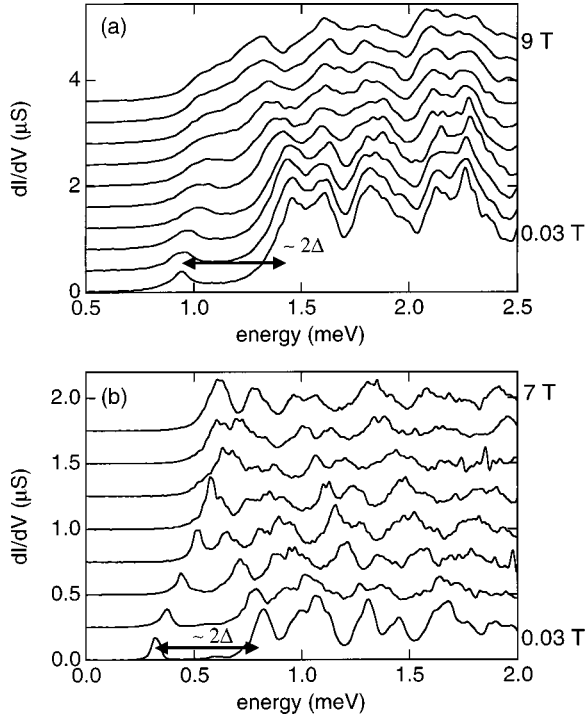


FIG. 5. (a) Tunneling spectrum for an Al particle containing 4% Au impurities, for a sequence of magnetic fields from 0.03 to 9 T in 1 T increments, $T = 15$ mK. The particle exhibits a superconducting gap for odd-to-even electron tunneling. (b) Comparison data for a pure Al particle, from Ref. 5. The curves are artificially offset for visibility.

the bare tunneling rates, of the type predicted by the spin-orbit scattering Hamiltonian. The lines in Figs. 3(b) and 3(c) display fits to the SO model result, Eq. (9), with only two adjustable parameters, $\Gamma_{L,a\uparrow}$, and $\Gamma_{L,b\downarrow}$, which simply set the $B=0$ values of the tunneling rates. For the slow-relaxation limit the B dependence of the tunneling rates is very well described by the SO formalism. In particular, as predicted by the model, the tunneling rates cross close to the same magnetic-field value, 5.4 T, where the avoided-crossing levels have their closest approach. Also, the tunneling rates well beyond the crossover regime are approximately equal to the $B=0$ tunneling rates. Neither result holds for the current increments themselves [Fig. 2(b)], due to the effect of the hidden levels. The agreement between the SO theory and the tunneling parameters estimated in the fast-relaxation limit is not quite as close as for the slow-relaxation limit. This is consistent with the estimates in Ref. 6 that the energy relaxation rate is 10^8 s^{-1} , an order of magnitude less than the tunneling rates we determine.

III. EFFECTS OF SPIN-ORBIT INTERACTIONS ON SUPERCONDUCTING NANOPARTICLES

We next consider different samples, a larger Al particle containing 4% Au impurities [Fig. 5(a)], compared to a pure Al particle of similar size showing no indications of SO scattering [Fig. 5(b)].²¹ Because of their larger size, the mean level spacings in both samples are smaller than in the device of Figs. 1–3, but nevertheless a large energy difference is visible between the first and second peaks in both spectra.

This is characteristic of odd-to-even tunneling in a superconducting particle. The energy gap reflects the large difference in energy (approximately twice the superconducting gap Δ) required for the tunneling of an electron to reach the ground state of an even-electron superconductor in which all electrons are paired, versus the first-excited state containing two unpaired quasiparticles.⁴ The two samples display qualitatively different behavior in a number of respects, however. One difference is that the resonance peaks in the Au-doped sample are somewhat broader. We believe that this is *not* related to the impurities, but is instead an effect of nonequilibrium distributions of electrons on the island,^{6,7} excited by a source-drain voltage three times larger than what is needed to overcome the Coulomb blockade and initiate tunneling in Fig. 5(a). Similar broadening could also be observed for the particle in Fig. 5(b) (see Ref. 5, Fig. 4), when a gate voltage was used to shift the tunneling spectrum to comparable values of the source-drain voltage. The device in Fig. 5(a) had no gate.

We will focus instead on the differences in the magnetic-field dependence of the data in Figs. 5(a) and 5(b). For the pure Al superconducting nanoparticle, the primary effect of a magnetic field is to produce linear shifts corresponding to a Zeeman spin splitting with $g_{\text{eff}} = 2 \pm 0.05$.²² The gap in the spectrum decreases linearly due to the difference in Zeeman energies for the ground and first-excited states of the superconductor, until it goes to zero at about 4 T. Models of superconductivity in small particles^{23,24} relate this crossing with the superconducting critical field, because the extent of electron pairing correlations drops abruptly at this point, although fluctuation-induced effects of attractive electron interactions may persist.²⁵ In contrast, all the resonance energies for the sample containing gold impurities are significantly less sensitive to an applied magnetic field. Instead of Zeeman splitting with $g_{\text{eff}} = 2$, the ground and first-excited-state transitions move at low B with slopes $g_{\text{eff},1}/2 + g_{\text{orb},1} = 0.41 \pm 0.03$ and $-g_{\text{eff},2}/2 + g_{\text{orb},2} = -0.27 \pm 0.03$, suggesting values for g_{eff} in the range 0.5–0.8. Even at 9 T, the gap between these states has not gone to zero, indicating a much larger critical field for superconductivity in this sample than for pure Al. Similar increases in critical fields due to the reduction in the effective g factor caused by SO scattering are familiar for thin films in parallel magnetic fields, and in other contexts where superconductivity is limited by spin-induced pair breaking.²⁶ At fields above 6 T, the slope of the energy vs B curve of the ground-state transition in the Au-doped sample changes sign (with the energy decreasing with increasing B at high fields), suggesting an avoided crossing with the higher-lying levels. The minimum gap between the ground-state and first-excited-state peaks corresponds to a SO matrix element of magnitude approximately $130 \mu\text{eV}$.²⁷

The presence of SO scattering must necessarily change the nature of the superconducting transition in a magnetic field. As we noted above for pure Al particles, the extent of superconducting pairing correlations is predicted to drop abruptly at the magnetic field for which the energy of the first state that moves to lower energy with increasing B (meaning that it is a spin-1 tunneling state) crosses below the energy of the upward-trending (spin-0) ground state, so that it becomes energetically favorable to break a Cooper pair. In

contrast, in the particles with significant SO scattering, the existence of avoided crossings means that energy levels corresponding to different spin states do not cross. Therefore the disruption of pairing correlations must occur gradually, as the spin content of the particle's ground state changes continuously in the avoided-crossing region.

Notably, the magnitude of the superconducting gap at $B = 0$ is not significantly affected by the presence of SO scattering. Setting the difference between the ground- and first-excited-state energies equal to 2Δ , $\Delta \approx 0.25$ meV for the pure Al particle of Fig. 5(b), similar to previous values,²⁸ and $\Delta \approx 0.26$ meV for the particle with Au impurities. This similarity is as expected, since SO scattering does not break time-reversal symmetry and therefore does not interfere with superconducting pairing.

IV. CONCLUSIONS

We have examined a number of effects associated with the presence of SO scattering in metal nanoparticles. The sensitivity of the “electron-in-a-box” energy levels to an applied magnetic field is weakened, so that they exhibit effective g values less than 2. When predominantly spin-up and spin-down levels approach each other as a function of magnetic field, they may undergo avoided crossings due to SO-induced coupling between the spin-up and spin-down states. In the avoided-crossing region, the magnitude of the current transported at the resonance thresholds can change, due to the changing admixture of spin-up and spin-down basis states that comprise the energy eigenstates. The presence of Au impurities does not greatly modify the size of the superconducting gap in Al particles large enough to exhibit

superconductivity. However, the critical magnetic field for the destruction of superconductivity is increased. We also argue that with the presence of SO scattering, the superconducting pairing parameter should vary continuously at large fields, because SO scattering eliminates the simple level crossings which cause the extent of pairing correlations to drop abruptly in pure Al samples. As a final remark, we note that all of the results that we describe can be adequately explained by treating the SO interaction perturbatively, and by ignoring the effect of the magnetic field on electron orbits. For samples with stronger SO interactions or with larger sizes such that effects of an applied field on the orbital states are significant, a more sophisticated treatment would be necessary.²⁹

Note added in proof. D. Davidovic and M. Tinkham have recently observed g factors reduced below 2 due to spin-orbit scattering in Au nanoparticles.³⁰

ACKNOWLEDGMENTS

We thank Leonid Glazman, Konstantin Matveev, and Jan von Delft for valuable discussions. The work at Cornell was supported by the MRSEC program of the NSF (Grant No. DMR-0632275), the Sloan Foundation, and the Packard Foundation, and was performed in part at the Cornell Nanofabrication Facility, funded in part by the NSF (Grant No. ECS-9319005), Cornell University, and industrial affiliates. The work at Harvard was supported by NSF Grant No. DMR-92-07956, ONR Grant No. N00014-96-1-0108, JSEP Grant No. N00014-89-J-1023, and ONR AASERT Grant No. N00014-94-1-0808.

¹For a review, see R. C. Ashoori, *Nature (London)* **379**, 413 (1996).

²M. A. Kastner, *Phys. Today* **46** (1), 24 (1993).

³D. C. Ralph, C. T. Black, and M. Tinkham, *Phys. Rev. Lett.* **74**, 3241 (1995).

⁴C. T. Black, D. C. Ralph, and M. Tinkham, *Phys. Rev. Lett.* **76**, 688 (1996).

⁵D. C. Ralph, C. T. Black, and M. Tinkham, *Phys. Rev. Lett.* **78**, 4087 (1997).

⁶O. Agam, N. S. Wingreen, B. L. Altshuler, D. C. Ralph, and M. Tinkham, *Phys. Rev. Lett.* **78**, 1956 (1997).

⁷O. Agam, and I. L. Aleiner, *Phys. Rev. B* **56**, R5759 (1997).

⁸G. Bergmann, *Phys. Rep.* **107**, 1 (1984).

⁹R. Meservey and P. M. Tedrow, *Phys. Rep.* **238**, 173 (1994).

¹⁰W. P. Halperin, *Rev. Mod. Phys.* **58**, 533 (1986).

¹¹J. A. A. J. Perenboom, P. Wyder, and F. Meier, *Phys. Rep.* **78**, 173 (1981).

¹²The spin-orbit scattering rate of interest for samples with a continuum density of states, $1/\tau_{\text{SO}}$, may be estimated (Ref. 10) in terms of a mean-squared spin-orbit matrix element and the mean level spacing δ :

$$\frac{1}{\tau_{\text{SO}}} \approx \frac{2\pi}{\hbar \delta} \overline{|H_{\text{SO}}|^2}.$$

For the data discussed in Figs. 1–3, the order of magnitude for this quantity is 10^{10} s^{-1} .

¹³C. T. Black, Ph.D. thesis, Harvard University, 1996.

¹⁴M. Hansen, *Constitution of Binary Alloys*, 2nd ed. (McGraw-Hill, New York, 1958).

¹⁵J. G. Lu, J. M. Hergenrother, and M. Tinkham, *Phys. Rev. B* **57**, 4591 (1998).

¹⁶We do not display $B=0$ data, because in this case the aluminum electrodes are superconducting, and this shifts the resonance peaks.

¹⁷An experimental upper bound on the shift in the average energies of Zeeman-split peaks in this sample would correspond to an effective orbital g factor less than 0.1. We are not able to comment on the functional form of any dependence of the orbital energy on magnetic field.

¹⁸V. Falko and K. Efetov, *Phys. Rev. B* **50**, 11 267 (1994).

¹⁹J. Sone, *J. Phys. Soc. Jpn.* **42**, 1457 (1977).

²⁰We will ignore shifting of the single-particle tunneling energies which may be produced by nonequilibrium electron occupations, producing clusters of tunneling resonances (Refs. 6 and 7), because these features are not resolved in this device.

²¹The data in Fig. 5(b) are from the same sample as the data in Figs. 2–4 of Ref. 5.

²²Claims of smaller g factors made in Ref. 4 are wrong, the result of confusing different orbital states as Zeeman-split spin states. This was made clear in Ref. 5, where we observed that upward-trending Zeeman states can have significantly smaller amplitude

than downward-trending states, making them difficult to observe.

- ²³F. Braun, J. von Delft, D. C. Ralph, and M. Tinkham, *Phys. Rev. Lett.* **79**, 921 (1997).
- ²⁴F. Braun and J. von Delft, *Phys. Rev. Lett.* **81**, 4712 (1998).
- ²⁵K. A. Matveev and A. I. Larkin, *Phys. Rev. Lett.* **78**, 3749 (1997).
- ²⁶A. M. Clogston, *Phys. Rev. Lett.* **9**, 266 (1962); B. S. Chandrasekhar, *Appl. Phys. Lett.* **1**, 7 (1962).
- ²⁷The estimate for this matrix element would be decreased if the lower-energy state is influenced by coupling to several higher-energy states in the avoided-crossing region.
- ²⁸Values quoted previously in Refs. 4 and 5 for Δ in pure Al particles, 0.29–0.38 meV, were determined in a slightly different way—by taking the difference between the low- B threshold for tunneling and the average threshold at high field where superconductivity is suppressed. Estimating 2Δ from the difference in energy between the two-quasiparticle state and the fully Cooper-paired state in an even-electron particle is expected to give a slightly smaller answer for Δ , because of gap suppression in the two-quasiparticle state.
- ²⁹L. Glazman (unpublished).
- ³⁰D. Davidovic and M. Tinkham, cond-mat/9905043 (unpublished).